Solar sail heliocentric transfers with a Q-law

Lorenzo Niccolai, Alessandro A. Quarta*, Giovanni Mengali

Dipartimento di Ingegneria Civile e Industriale, University of Pisa, Italy

Abstract

The propellantless working principle of a solar sail requires the total flight time to be minimized when looking for the optimal trajectory to reach a given target state. In this work the solar sail steering law is found by applying a Q-law algorithm, which aims at driving the spacecraft towards the final (target) orbit by decreasing the distance between actual and desired states or by increasing the rate of change of the state variables. A formulation of the Q-law algorithm for a solar sail-based mission is given, which accounts for the constraints along the transfer trajectory imposed by the sail thrust model. The performance of the proposed procedure, which represents the novelty of this work, is checked in some potential solar sail mission scenarios, including coplanar interplanetary transfers and the exploration of outer Solar System regions.

Keywords: solar sail, Q-law, interplanetary transfer, outer Solar System exploration

Nomenclature

a	=	osculating orbit semimajor axis, [au]
$\widetilde{a}$	=	dimensionless osculating orbit semimajor axis
a_c	=	characteristic acceleration, [$\mathrm{mm/s^2}$]
a_{PR}	=	radial component of the propulsive acceleration, [$\mathrm{mm/s^2}$]
a_{PT}	=	transverse component of the propulsive acceleration, [$\mathrm{mm/s^2}$]
C	=	penalty function dimensionless constant, see Eq. (14)
$\{c_1, c_2, c_3\}$	=	scaling function dimensionless constants, see Eq. (13)
e	=	osculating orbit eccentricity
h	=	angular momentum vector magnitude, [$\mathrm{km^2/s}$]
$\{K, k\}$	=	auxiliary constants, see Eqs (25)-(26) and (32)-(33)
O	=	Sun's center-of-mass
$\text{œ} = \{\widetilde{a},\, e,\, \omega\}$	=	orbital element
œ_{xx}	=	maximum time derivative of œ over α and ν, see Eq. (15)
P	=	penalty function, see Eq. (14)
p	=	osculating orbit semilatus rectum, [au]
Q	=	proximity quotient, see Eq. (12)
r	=	Sun-spacecraft distance, [au]
r_p	=	perihelion distance, [au]
S	=	scaling function, see Eq. (13)
$\mathcal{T}(O; r,\, \theta)$	=	heliocentric polar reference frame
t	=	time, [days]
u	=	radial component of the spacecraft velocity, [km/s]

*Corresponding author

Email addresses: lorenzo.niccolai@ing.unipi.it (Lorenzo Niccolai), a.quarta@ing.unipi.it (Alessandro A. Quarta), g.mengali@ing.unipi.it (Giovanni Mengali)

Published in Acta Astronautica, Vol. 188, November 2021, pp. 352–361. doi: https://doi.org/10.1016/j.actaastro.2021.07.037

v	=	transverse component of the spacecraft velocity, [km/s]
W_i	=	weight associated with variable or function i
α	=	thrust angle, [deg]
α_i	=	candidate optimal pitch angle, see Eqs. (35)–(40), [deg]
ϵ	=	dimensionless error, see Eq. (43)
θ	=	polar angle, [deg]
$\mu_\odot$	=	Sun's gravitational parameter, [$\mathrm{km}^3/\mathrm{s}^2$]
ν	=	true anomaly, [deg]
ω	=	osculating orbit argument of perihelion, [deg]

Subscripts

$\oplus$	=	Earth
end	=	end of the integration
min	=	minimum value
0	=	initial value
f	=	final (terminal) condition
œ	=	associated with orbital element œ
opt	=	optimal value
R	=	associated with radial component
T	=	associated with transverse component

Superscripts

$\cdot$	=	time derivative
$-$	=	auxiliary variable

1. Introduction

Solar sails are innovative propellantless propulsive systems that exploit the momentum exchange between the incoming photons from the Sun and a thin membrane [1, 2, 3], or several reflective and spinning blades [4], to generate thrust. Although the existence of solar radiation pressure has been known for a long time, the recent successes of solar sail-based missions, such as IKAROS [5, 6], LightSail-1 [7] and LightSail-2 [8], have given a renewed impulse to the technological development of the solar sail concept. For example, refractive and diffractive sails have been recently proposed, which are capable of generating an in-plane transverse thrust even in a Sun-facing configuration [9, 10]. The interest of the scientific community on solar sailing has led to the design of several solar sail-based missions, including NASA's NEA Scout [11], Solar Cruiser [12], and JAXA's OKEANOS [13, 14], which require a deep space transfer phase to reach the target position or the working orbit.

The propellantless working principle of solar sails requires that the optimal solar sail-propelled trajectory is the solution of a minimum-time problem with prescribed values of initial and final spacecraft states. The spacecraft trajectory is obtained by suitably adjusting the sail attitude along the transfer, and many strategies exist in the literature for calculating the time-optimal steering law. These methods may be grouped in either global or local approaches, where global optimization algorithms aim at finding the global minimum of the transfer time and the corresponding steering law. Global strategies include indirect methods [15, 16, 17, 18, 19, 20], and direct methods, such as pseudospectral methods [21], nonlinear programming [22, 23], a combination of genetic algorithms and quadratic programming [24], and shape-based methods [25]. In this context, a comparison between the performance of direct and indirect approaches for solar sail trajectory optimization has been recently analyzed in Ref. [26]. Other more complex global optimization techniques have been proposed in the literature, including the evolutionary neurocontrol by Dachwald [27], or the use of deep neural networks, first used for trajectory optimization of low-thrust spacecraft with conventional engines [28], and applied to solar sail-based mission scenarios [29, 30]. Locally-optimal approaches, instead, aim at minimizing (or maximizing), at each time instant, a given performance index, usually the time

derivative of an orbital parameter or a linear combination of the time derivatives of two or more osculating orbital elements [31, 32, 33].

An example of locally-optimal strategy for determining the time-optimal control law of a low-thrust-propelled spacecraft is the Q-law, first proposed by Petropoulos [34] about 20 years ago. This algorithm, which is a refined local-optimization technique, is based on the definition of a nonnegative dimensionless proximity quotient Q, the time derivative of which has to be minimized at each time. The distinguishing characteristics and the main advantages of a Q-law algorithm with respect to other optimization techniques are in its simplicity and small computational cost it requires. Indeed, a Q-law algorithm essentially relies on analytical approximated mathematical expressions and, unlike most (especially global) optimization methods, it does not require any initial guess of the solution.

In particular, the dimensionless proximity quotient Q is an increasing function of the Euclidean distance between the instantaneous and the target spacecraft state, and a decreasing function of the maximum time derivatives of the state variables, that is, the osculating orbital parameters. With such a definition of the proximity quotient Q, a reduction of its value may be obtained either by reducing the difference between the osculating orbit elements and the target elements, or by increasing the maximum variation rate of the orbital parameters. The performance of a Q-law algorithm has been investigated in several mission scenarios based on conventional low-thrust propulsive systems (mainly electric thrusters), and the original algorithm has been also refined to include the possible presence of coasting arcs along the trajectory [35], or to account for orbital perturbations (such as the Earth's oblateness) and eclipse periods in planetocentric mission scenarios [36, 37, 38]. The solutions provided by the Q-law algorithm have also been used as first guesses for global optimization algorithms to reduce the total computation time [39, 40, 41, 42].

The aim of this work (and its new contribution) consists in adapting the Q-law algorithm formulation to the case of a solar sail-based spacecraft. Unlike the propulsive acceleration generated by a conventional electric thruster, the magnitude of the sail thrust vector scales as the inverse square heliocentric distance, and its components are functions of the sail attitude. The solar sail trajectory generated by a Q-law algorithm will be tested in two mission scenarios, that is, a coplanar circle-to-circle interplanetary rendezvous [15], and a mission toward the outer regions of the Solar System [27, 43, 44, 45]. The latter case is especially well suited for solar sail-based spacecraft, which may exploit one (or more) solar photonic assist maneuvers, consisting in a close passage near the Sun to exploit the gravity assist and the increased solar radiation pressure [46, 47]. This maneuver is very useful for low- and medium-performance solar sails, and optimal trajectories with single or multiple photonic assists are usually difficult to find with conventional optimization algorithms [48].

The rest of the manuscript is structured as follows. Section 2 describes the dynamical model of the problem, while Section 3 discusses the specific formulation of the Q-law algorithm for a spacecraft propelled by an ideal solar sail. The proposed procedure is tested in Section 4 with the aid of two mission scenarios, and the outputs are compared with results taken from the recent literature. Finally, the Conclusion section summarizes the outcomes of this analysis.

2. Mathematical model

Consider a heliocentric two-dimensional trajectory of a solar sail-based spacecraft, in which the propulsive acceleration vector always lies on the parking orbit plane. Introduce a polar reference frame $\mathcal{T}(O; r, \theta)$, with its origin O coincident with the Sun's center of mass, as is sketched in Fig. 1. In that scenario, the spacecraft dynamics are described by the classical equations of motion

$$\dot{r} = u \tag{1}$$

$$\dot{\theta} = \frac{v}{r} \tag{2}$$

$$\dot{u} = \frac{v^2}{r} - \frac{\mu_\odot}{r^2} + a_{PR} \tag{3}$$

$$\dot{v} = -\frac{u\,v}{r} + a_{PT} \tag{4}$$

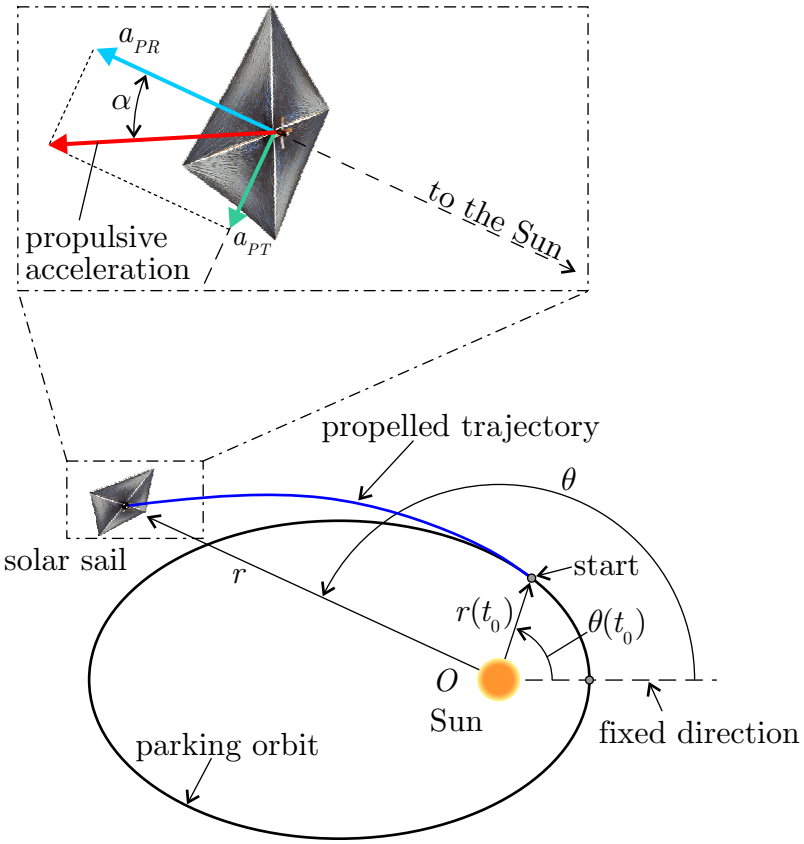

Figure 1: Sketch of the polar reference frame and of the propulsive acceleration components used to formulate the mathematical model.

where r is the Sun-spacecraft distance, θ is the polar angle measured counterclockwise from a fixed direction, $\mu_\odot$ is the Sun's gravitational parameter, u (or v) is the radial (or transverse) component of the spacecraft inertial velocity, and a_{PR} (or a_{PT}) is the radial (or transverse) component of the sail propulsive acceleration vector. The osculating orbital elements may be calculated from the spacecraft state variables $\{r, \theta, u, v\}$ using the expressions

$$a = \left(\frac{2}{r} - \frac{u^2 + v^2}{\mu_\odot} \right)^{-1} \tag{5}$$

$$e = \sqrt{1 - \frac{r^2 \, v^2}{\mu_\odot \, a}} \tag{6}$$

$$\nu = \text{sign}\,(u) \arccos \left\{ \frac{1}{e} \left[\frac{a(1-e^2)}{r} - 1 \right] \right\} \tag{7}$$

$$\omega = \theta - \nu + \omega_0 \tag{8}$$

where a is the semimajor axis, e is the eccentricity, ν is the true anomaly, and ω is the osculating orbit apse line rotation angle, while the subscript 0 refers to the initial time $t = 0$. To account for both closed and open osculating orbits, the convention according to which $\nu \in [-\pi, \pi]$ rad has been adopted in Eq. (7). Note that the orbital elements calculated with Eqs. (5)–(8) will be used in the rest of the paper to define the Q-law algorithm.

The components of the solar sail propulsive acceleration vector vary according to the various thrust

models available in the literature [49]. The ideal force model, which assumes each photon impinging on the (flat) sail film to be specularly reflected, will be used in this work. In fact, such a model provides sufficiently accurate results for the purposes of a preliminary mission analysis at a low computational effort, and allows the outputs of the numerical simulations to be compared with those found in the literature. Other, more complex, sail thrust models exist, which take into account the optical properties of the reflective film [19], the degradation of the sail surface [50, 51], the sail billowing [2], or the presence of wrinkles [52, 53].

The components of the ideal sail propulsive acceleration vector $\{a_{PR}, a_{PT}\}$ are given by [1, 2]

$$a_{PR} = a_c \left(\frac{r_\oplus}{r}\right)^2 \cos^3\alpha \tag{9}$$

$$a_{PT} = a_c \left(\frac{r_\oplus}{r}\right)^2 \cos^2\alpha \sin\alpha \tag{10}$$

where $r_\oplus \triangleq 1\,\text{au}$ is a reference distance, and a_c is the spacecraft characteristic acceleration, that is, the maximum propulsive acceleration magnitude at $r = r_\oplus$. In Eqs. (9)-(10), the term $\alpha \in [-\pi/2, \pi/2]\,\text{rad}$ is the thrust angle, defined as the angle (measured counterclockwise along the parking orbit plane) between the Sun-spacecraft line and the thrust vector direction, see Fig. 1. The thrust angle may be calculated as

$$\alpha = \arctan\left(\frac{a_{PT}}{a_{PR}}\right) \tag{11}$$

In an ideal force model the thrust angle α coincides with the sail pitch angle, that is, the angle between the external normal to the sail nominal plane and the radial direction [2]. Note that the thrust vector cannot be freely oriented, as is shown in Fig. 2, where the straight lines report the values of the thrust angle.

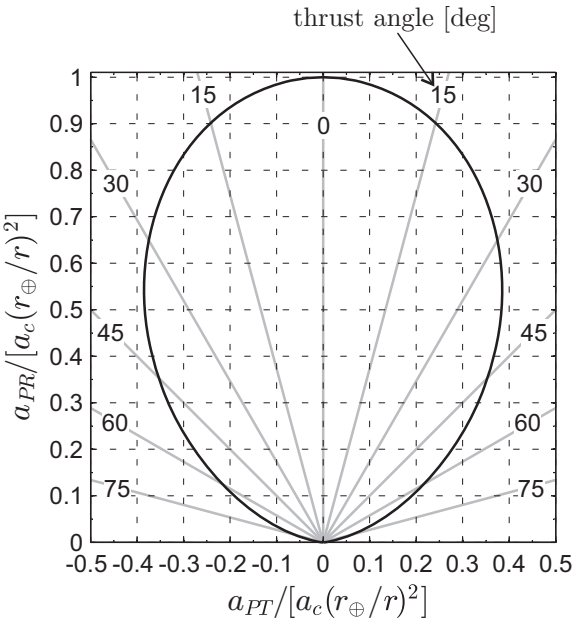

Figure 2: Dimensionless components of the ideal (flat) sail propulsive acceleration vector.

As is usual in solar sail trajectory analysis, the time-variation of the thrust angle $\alpha = \alpha(t)$ is designed to allow a spacecraft to move from a set of initial conditions $\{r(t_0),\, \theta(t_0),\, u(t_0),\, v(t_0)\}$ (see Fig. 1) to a final (target) state, by minimizing the total flight time. The target state is fully described by a given set of state variables $\{r(t_f),\, \theta(t_f),\, u(t_f),\, v(t_f)\}$ where t_f is the final time instant, although, some of the terminal conditions may not be specified a priori.

3. Q-law algorithm application to solar sail transfer trajectories

We now illustrate a procedure to approximate the minimum-time solar sail trajectory with a Q-law algorithm, in which a dimensionless proximity quotient Q is used to quantify the differences between the osculating and the target orbit (dimensionless) parameters $\text{œ} \in \{\widetilde{a},\, e,\, \omega\}$ with $\widetilde{a} \triangleq a/a_0$, where a_0 is the (parking) orbit semimajor axis at $t = 0$. To simplify the analysis, and in analogy with Refs. [34, 35, 42], assume that Q is independent of ν, which amounts to state that the target true anomaly is left unconstrained.

In this context, the proximity quotient Q is defined as

$$Q \triangleq (1 + W_P\, P) \sum_{\text{œ}} W_{\text{œ}}\, S_{\text{œ}} \left(\frac{\text{œ} - \text{œ}_f}{\dot{\text{œ}}_{xx}} \right)^2 \tag{12}$$

where the subscript f refers to the target (final) value, $W_i \geq 0$ is a dimensionless weight parameter related to the generic variable i, and $S_{\text{œ}}$ is a dimensionless scaling function, used to prevent a non-convergence to the target state [35, 42]. In particular, the generic $S_{\text{œ}}$ is defined as

$$S_{\text{œ}} = \begin{cases} \left[1 + \left(\dfrac{a - a_f}{c_1\, a_f} \right)^{c_2} \right]^{\frac{1}{c_3}} & \text{for } \text{œ} = \widetilde{a} \\ 1 & \text{for } \text{œ} \in \{e,\, \omega\} \end{cases} \tag{13}$$

where $\{c_1, c_2, c_3\}$ are dimensionless tuning parameters, of which the suggested values [35] are $c_1 = 3$, $c_2 = 4$, and $c_3 = 2$. The term P in Eq. (12) is a penalty function, used to enforce a constraint on the minimum perihelion radius $r_{p_{\min}}$ to avoid a close approach to the Sun, and defined as

$$P \triangleq \exp\left[C \left(1 - \frac{a\,(1 - e)}{r_{p_{\min}}} \right) \right] \tag{14}$$

where the C is a dimensionless tuning parameter. Finally, the terms $\dot{\text{œ}}_{xx} \in \{\dot{\widetilde{a}}_{xx},\, \dot{e}_{xx},\, \dot{\omega}_{xx}\}$ in Eq. (12) are defined as

$$\dot{\text{œ}}_{xx} \triangleq \max_{\nu,\alpha} (\dot{\text{œ}}) \tag{15}$$

and represent the maximum value of the time-derivative of the generic (dimensionless) orbital parameter œ that may be achieved along the osculating orbit by suitably steering the sail nominal plane.

In particular, the terms $\dot{\text{œ}}_{xx}$ may be estimated starting from the Gauss' variational equations, which provide the time derivatives of the osculating orbital elements as functions of the components of the propulsive acceleration vector $\{a_{PR}, a_{PT}\}$, viz.

$$\frac{\mathrm{d}\widetilde{a}}{\mathrm{d}t} = \frac{2\,a^2}{h\,a_0} \left[e\, \sin\nu\, a_{PR} + (1 + e\, \cos\nu)\, a_{PT} \right] \tag{16}$$

$$\frac{\mathrm{d}e}{\mathrm{d}t} = \frac{1}{h} \{ p\, \sin\nu\, a_{PR} + [(p + r)\, \cos\nu + e\, r]\, a_{PT} \} \tag{17}$$

$$\frac{\mathrm{d}\omega}{\mathrm{d}t} = \frac{1}{e\, h} \left[-p\, \cos\nu\, a_{PR} + (p + r)\, \sin\nu\, a_{PT} \right] \tag{18}$$

where $p \triangleq a(1 - e^2)$ is the osculating orbit semilatus rectum, $h \triangleq \sqrt{\mu_\odot\, p}$ is the angular momentum vector magnitude, and $\{a_{PR}, a_{PT}\}$ are given by Eqs. (9)-(10). Starting from Eqs. (16)–(18), in principle the values of the coefficients $\dot{\text{œ}}_{xx}$ may be found with an analytical or a numerical approach. However, to simplify the problem and in analogy with Refs. [34, 35, 42], the values of $\dot{\text{œ}}_{xx}$ will be calculated with suitable approximate analytical expressions.

More precisely, according to Ref. [35], $\dot{\widetilde{a}}_{xx}$ may be estimated by observing that the maximum variation of the semimajor axis is obtained by applying the maximum transverse component of the propulsive acceleration at the osculating orbit pericenter (i.e., at $\nu = 0$ and $r = a - ae$). When such a strategy is specialized to a

solar sail-based spacecraft, Eq. (10) shows that the thrust angle that maximizes the transverse component a_{PT} is $\alpha^\star \triangleq \arcsin(1/\sqrt{3})\,\text{rad}$. The term $\dot{\widetilde{a}}_{xx}$ is therefore written by enforcing the conditions

$$r = a\,(1-e) \quad , \quad \nu = 0 \quad , \quad \alpha = \alpha^\star \tag{19}$$

into Eqs.(9)-(10) and (16). Recalling that $\sin\alpha^\star = 1/\sqrt{3}$ and $\cos\alpha^\star = \sqrt{2/3}$, the result is

$$\dot{\widetilde{a}}_{xx} = \frac{4}{3\,a_0\,\sqrt{3}}\,\sqrt{\frac{1+e}{\mu_\odot\,a\,(1-e)^5}}\,a_c\,r_\oplus^2 \tag{20}$$

An analytical expression of $\dot{e}_{xx}$ cannot be retrieved for a solar sail-based spacecraft, but an approximate expression may be found by assuming that the maximum value of $\dot{e}$ is approximately obtained at the perihelion of the osculating orbit with a thrust angle equal to $\alpha^\star$, that is, using the maximum transverse component of the propulsive acceleration, viz.

$$\dot{e}_{xx} = \frac{4}{3\,\sqrt{3}}\,\sqrt{\frac{1+e}{\mu_\odot\,a^3\,(1-e)^3}}\,a_c\,r_\oplus^2 \tag{21}$$

Likewise, $\dot{\omega}_{xx}$ cannot be calculated in an exact form, but may be approximated with similar considerations as

$$\dot{\omega}_{xx} = \frac{4}{3\,p\,e\,h\,\sqrt{3}}\,a_c\,r_\oplus^2 \tag{22}$$

which comes from Eq. (18) with the aim of maximizing the (positive) contribution to the propulsive acceleration from the transverse component, that is, by enforcing the conditions $\nu = \pi/2\,\text{rad}$ and $\alpha = \alpha^\star$. The results from Eqs. (20)–(22) are illustrated in Fig. 3 as a function of $\{a, e\}$ assuming $a_c = 0.5\,\text{mm/s}^2$ and $a_0 = r_\oplus$.

The time derivative of the proximity quotient Q is given by

$$\dot{Q} = \sum_{\text{œ}} \frac{\partial Q}{\partial \text{œ}}\,\dot{\text{œ}} \tag{23}$$

where the analytical expression of $\partial Q/\partial$œ, which may be calculated from Eq. (12), is not reported here for the sake of conciseness. The Q-law algorithm requires $\dot{Q}$ to be minimized. To that end, first note that

$$\dot{\text{œ}} = k_{\text{œ}_R}\,a_{PR} + k_{\text{œ}_T}\,a_{PT} \tag{24}$$

where

$$k_{\text{œ}_R} \triangleq \frac{\partial \dot{\text{œ}}}{\partial a_{PR}} \tag{25}$$

$$k_{\text{œ}_T} \triangleq \frac{\partial \dot{\text{œ}}}{\partial a_{PT}} \tag{26}$$

may be written as a function of the osculating orbit parameters through the Gauss' variational equations (16)–(18). Substituting Eq. (24) into Eq. (23) yields

$$\dot{Q} = \sum_{\text{œ}} \left[\frac{\partial Q}{\partial \text{œ}}\,(k_{\text{œ}_R}\,a_{PR} + k_{\text{œ}_T}\,a_{PT})\right] \tag{27}$$

where the propulsive acceleration components $\{a_{PR}, a_{PT}\}$ are functions of the control variable α and the Sun-spacecraft distance r. Define now the equivalent propulsive acceleration components $\{\overline{a}_{PR}, \overline{a}_{PT}\}$ as

$$\overline{a}_{PR} \triangleq a_{PR}\left(\frac{r}{r_\oplus}\right)^2 = a_c\,\cos^3\alpha \tag{28}$$

$$\overline{a}_{PT} \triangleq a_{PT}\left(\frac{r}{r_\oplus}\right)^2 = a_c\,\cos^2\alpha\sin\alpha \tag{29}$$

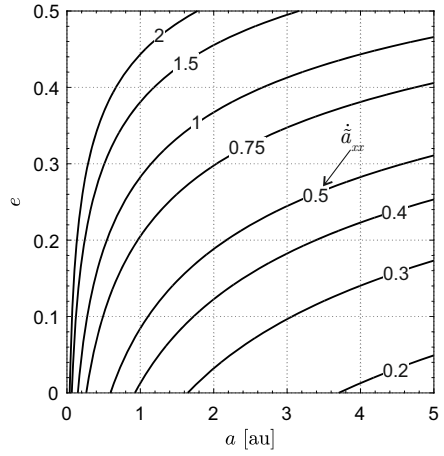

(a) $\dot{\tilde{a}}_{xx}$

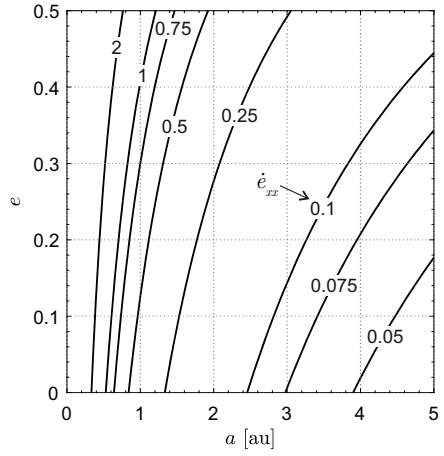

(b) $\dot{e}_{xx}$

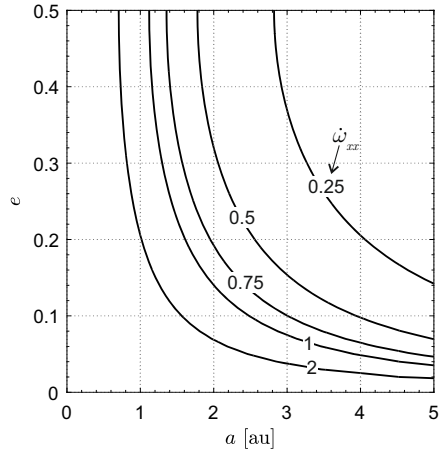

(c) $\dot{\omega}_{xx}$

Figure 3: Contours of $\dot{\mathrm{e}}_{xx} \in \{\dot{\tilde{a}}_{xx}, \dot{e}_{xx}, \dot{\omega}_{xx}\}$ as functions of a and e when $a_c = 0.5\,\mathrm{mm/s^2}$ and $a_0 = r_\oplus$.

which depend on the sail attitude only through the thrust angle α. Substituting Eqs. (28)-(29) into Eq. (24) we get

$$\dot{\text{œ}} = \frac{k_{\text{œ}_R}}{(r/r_\oplus)^2}\,\overline{a}_{PR} + \frac{k_{\text{œ}_T}}{(r/r_\oplus)^2}\,\overline{a}_{PT} \tag{30}$$

Combining Eq. (30) with Eq. (27) and paralleling the approach discussed in Ref. [42], the time derivative of the proximity quotient Q is written as

$$\dot{Q} = K_R\,\cos\alpha^3 + K_T\,\cos\alpha^2\,\sin\alpha \tag{31}$$

with

$$K_R \triangleq a_c\,\left(\frac{r_\oplus}{r}\right)^2 \sum_{\text{œ}} \frac{\partial Q}{\partial \text{œ}} k_{\text{œ}_R} \tag{32}$$

$$K_T \triangleq a_c\,\left(\frac{r_\oplus}{r}\right)^2 \sum_{\text{œ}} \frac{\partial Q}{\partial \text{œ}} k_{\text{œ}_T} \tag{33}$$

where $\{k_{\text{œ}_R},\, k_{\text{œ}_T}\}$ are given by Eqs. (25)-(26). Since the derivatives of the proximity quotient with respect to the orbital parameters may be analytically calculated, the pair $\{K_R,\, K_T\}$ is easily obtained at each time instant along the transfer trajectory. The minimum of $\dot{Q}$ is therefore a function of the thrust angle α only, so that the stationary points of Eq. (31) are given by

$$\frac{\partial \dot{Q}}{\partial \alpha} = 0 \qquad \text{with} \qquad \alpha \in \{\alpha_1, \alpha_2, \alpha_3, \alpha_4\} \tag{34}$$

where

$$\alpha_1 \triangleq \arcsin\left(\sqrt{\frac{3\,K_R^2 - 3\,K_R\,\sqrt{K_R^2 + \frac{8}{9}\,K_T^2} + 2\,K_T^2}{6\,K_R^2 + 6\,K_T^2}}\right) \tag{35}$$

$$\alpha_2 \triangleq \arcsin\left(\sqrt{\frac{3\,K_R^2 + 3\,K_R\,\sqrt{K_R^2 + \frac{8}{9}\,K_T^2} + 2\,K_T^2}{6\,K_R^2 + 6\,K_T^2}}\right) \tag{36}$$

$$\alpha_3 \triangleq -\alpha_1 \tag{37}$$

$$\alpha_4 \triangleq -\alpha_2 \tag{38}$$

Note that the set of stationary points must be completed with

$$\alpha_5 = \pi/2\,\text{rad} \tag{39}$$

$$\alpha_6 = -\pi/2\,\text{rad} \tag{40}$$

which correspond to the boundaries of the variation range of the thrust angle. The set of candidates points is therefore

$$\mathfrak{I}_\alpha \triangleq \{\alpha_1,\, \alpha_2,\, \alpha_3,\, \alpha_4,\, \alpha_5,\, \alpha_6\} \tag{41}$$

and the optimal thrust angle α_{opt} results from

$$\alpha_{\text{opt}} = \arg\min_{\alpha \in \mathfrak{I}_\alpha} \dot{Q}(\alpha) \tag{42}$$

where $\dot{Q}$ is given by Eq. (31), and the angles $\alpha_i \in \mathfrak{I}_\alpha$ are calculated from Eqs. (35)–(40).

Having obtained the optimal thrust angle from Eq. (42), the corresponding propulsive acceleration components come from Eqs. (9)-(10), and the spacecraft dynamics are simulated by (numerically) integrating Eqs. (1)–(4) to avoid singularities. In this analysis it is assumed that the optimal thrust angle may always be achieved, without considering possible constraints on solar sail attitude. The interested reader is referred to the recent paper by Caruso et al. [25] for an in depth discussion on this last topic.

4. Case study and simulation results

The proposed Q-law algorithm has been simulated in some typical heliocentric mission cases, which represent potential mission applications for a solar sail-based spacecraft. Depending on the different mission requirements, the Q-law algorithm has been suitably tuned to maximize its performance.

4.1. Coplanar interplanetary transfers

The first group of mission cases concerns a classical interplanetary transfer towards Mars or Venus. Considering a two-dimensional motion, the relative inclination between the planetary orbits is neglected, and the orbits of Earth, Mars, and Venus are all supposed to be circular, that is, $e_0 \equiv e_f = 0$. It is assumed that the solar sail leaves the Earth's sphere of influence following a parabolic escape trajectory with zero hyperbolic excess velocity relative to the planet, so that at time t_0, when the transfer starts, the spacecraft osculating orbit parameters are those of the Earth (i.e., $a_0 = r_\oplus$). The mission aim is to perform an orbit-to-orbit transfer, by matching the semimajor axis and eccentricity of the target planet, with no constraint on planetary ephemerides. Accordingly, in a circle-to-circle orbit transfer the only relevant parameters are a and e, so that the weight related to the argument of pericenter is set equal to zero, that is, the condition $W_\omega = 0$ is enforced in Eq. (12).

The Q-law algorithm does not impose any boundary constraint on the spacecraft trajectory, so it may only ensure an asymptotic convergence towards the target state, before the eventual onset of numerical errors. The Euclidean distance from the target orbit is measured by a dimensionless error ϵ, defined as

$$\epsilon \triangleq \sqrt{\frac{(a - a_f)^2}{a_f^2} + e^2} \tag{43}$$

where the orbital parameters $\{a, e\}$ in Eq. (43) are calculated at the time instant when the numerical integration of the equations of motion is stopped. In the simulated scenarios, the maximum value of ϵ required for convergence is 5×10^{-2} in the Earth-Venus transfer, and of 10^{-1} in the Earth-Mars case. Since trajectories with a convergence error close to the maximum allowable values require small corrective maneuvers to reach the target orbit, they are well suited for estimating the required transfer time and may be used as first guesses for more refined optimization procedures. On the contrary, values of ϵ on the order of 5×10^{-2} or smaller are considered to be satisfactory, and correspond to trajectories that actually accomplish an interplanetary orbit-to-orbit transfer.

The first test case is an Earth-Venus orbit-to-orbit circular transfer, with $a_f = 0.723\,\text{au}$. According to Ref. [42], the weights of the two state variables a and e are chosen within the range $W_a \in [1, 10]$ and $W_e \in [1, 10]$. The minimum perihelion constraint is set to $r_{p_{\min}} = 0.2\,\text{au}$, with a value $C = 100$ in the penalty function of Eq. (14) (although it is inactive in all of the simulated trajectories). Among the possible transfer trajectories, the optimal solution for each value of the characteristic acceleration a_c is chosen as the one that minimizes the value of ϵ.

The flight times to Venus are reported in Fig. 4, which shows a very good accordance with the results (in red colour) taken from the global optimization algorithm discussed in Refs. [54, 55]. The convergence errors are very satisfactory, with a mean value of 1.4×10^{-2} for the trajectories shown in Fig. 4. An example of an Earth-Venus transfer trajectory (assuming $a_c = 0.5\,\text{mm/s}^2$) along with the required steering law $\alpha = \alpha(t)$ is illustrated in Fig. 5. The convergence dimensionless error in this case is $\epsilon = 3.4 \times 10^{-3}$.

The second test case is an Earth-Mars circular transfer, with $a_f = 1.523\,\text{au}$. The weights W_a and W_e are chosen to vary within the same range as that in the Earth-Venus scenario, and the constraint on the minimum perihelion radius is, again, inactive. In this case the convergence errors are higher than those of the Earth-Venus transfer, and the maximum convergence error is set equal to 10^{-1}. This means that

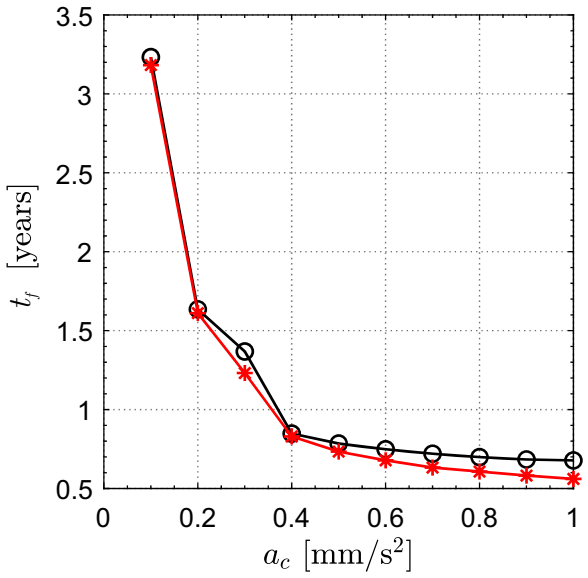

Figure 4: Earth-Venus flight times t_f as a function of a_c (black dots = Q-law algorithm, red asterisks = global optimal).

in most cases the Q-law algorithm only gives a rough estimation of the optimal transfer trajectory, which could be used as an initial guess for a succeeding optimization algorithm, in analogy with what suggested by Refs. [39, 40, 41, 42].

In this context, Fig. 6 shows the resulting Earth-Mars estimated flight times, which are similar to those obtained with the global optimization algorithm discussed in Refs. [54, 55]. The Earth-Mars transfers have dimensionless errors with a mean value of 5×10^{-2}. Figure 7 illustrates the Earth-Mars transfer trajectory with $a_c = 0.3\,\mathrm{mm/s^2}$ and $\epsilon = 8.2 \times 10^{-3}$, together with the corresponding steering law $\alpha = \alpha(t)$.

4.2. Missions to the outer Solar System

Advanced mission scenarios regarding the exploration of the outer Solar System have been often proposed for spacecraft with propellantless propulsion systems [17, 27, 44, 45, 56]. The main mission objectives usually include a flyby with a distant planet or require to reach the heliopause region to obtain *in-situ* observations of the interstellar medium. In all cases, a large heliocentric distance r_f must be bridged within a reasonable flight time. In principle, the Sun-spacecraft distance is a function of a, e, and ν, although a fast transfer can be approximated with a rapid growth of the spacecraft orbital energy, that is, by increasing the value of a. This approximation is supported by the fact that trajectories toward the outer Solar System region must achieve large values of the mechanical energy, as is discussed in Ref. [57]. Therefore, apart from W_a, the other two weights of the Q-law algorithm are both chosen to be zero, that is, $W_e = W_\omega = 0$ in Eq. (12).

The definition of Q requires the target orbital elements to be specified. The semimajor axis is set equal to the target distance ($a_f = r_f$), but such a choice would cause the algorithm to convergence to a target state with $r < r_f$. Therefore, as soon as the aphelion radius of the osculating orbit reaches the target radius, that is, $a(1+e) = r_f$, the Q-law algorithm is no more used to steer the solar sail. Since the orbital energy is now sufficient to reach the target distance, the solar sail must increase as quickly as possible its heliocentric distance. To do so, a steering law that maximizes the transverse component a_{PT} of the propulsive acceleration is enforced, which amounts to set $\alpha = \alpha^\star$; see Eq. (10). In conclusion, the Q-law algorithm with $a_f = r_f$ is used as long as the condition $a(1+e) = r_f$ is met, from then on a constant thrust angle $\alpha = \alpha^\star$ is assumed.

As previously stated, the optimal trajectory for a solar sail to reach the outer Solar System region usually requires one (or more) photonic assist maneuvers. As is sketched in Fig. 8, such a maneuver consists in a passage close to the Sun in order to exploit the increased Sun's gravity and solar radiation pressure to increase its orbital energy [46, 47]. The constraint on the minimum perihelion distance expressed by the penalty function in Eq. (14) obviously plays a crucial role in the resulting trajectories, so that different

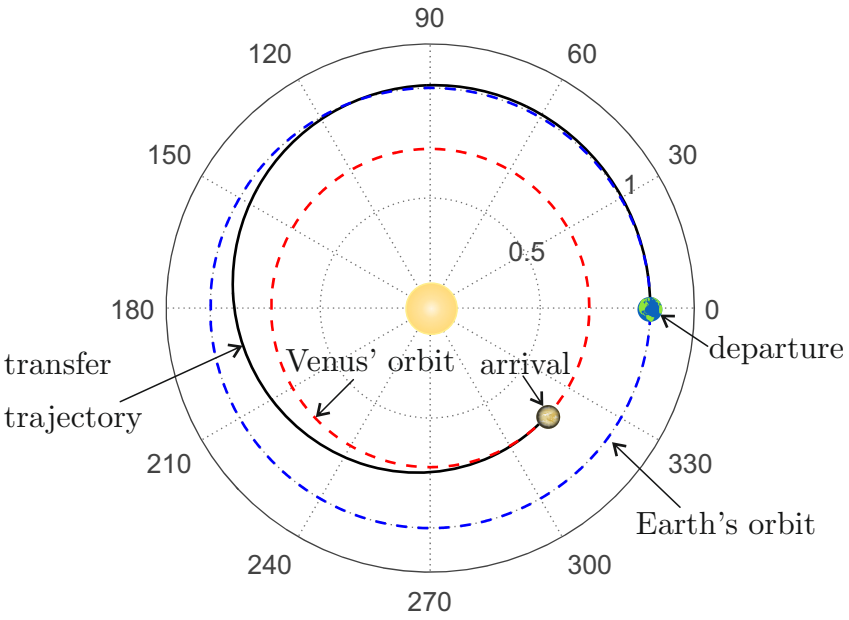

(a) Transfer trajectory. Radial distance in astronomical units.

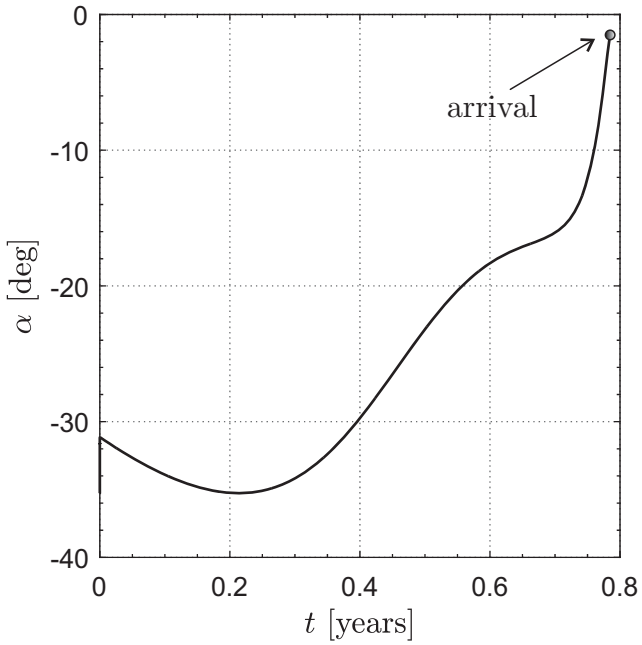

(b) Steering law.

Figure 5: Earth-Venus transfer trajectory when $a_c = 0.5\,\mathrm{mm/s^2}$.

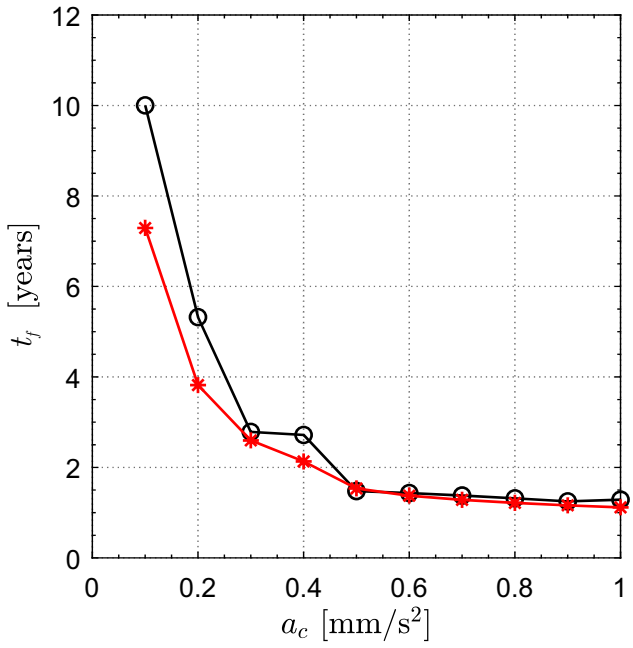

Figure 6: Earth-Mars flight times t_f as a function of the characteristic acceleration a_c (black dots = Q-law algorithm, red asterisks = global optimal).

values have been considered in the simulations, that is, $r_{p_{\min}} \in \{0.1, 0.2, 0.3, 0.4, 0.5\}$ au. The unconstrained trajectory is first obtained by setting $W_P = 0$ in Eq. (14), while the other cases are simulated with $W_P = 1$ and using the specific value of $r_{p_{\min}}$. In all cases, it is assumed that $C = 100$ in Eq. (14).

The test case chosen in the simulations is an orbital flyby with Neptune. Neglecting the planetary ephemeris, the problem is to reach a target heliocentric distance of $r_f = 30$ au. The flight times are reported in Tab. 1 as a function of the minimum perihelion distance and characteristic acceleration $a_c \in \{0.5, 1, 2\}$ mm/s^2. The inner part of the transfer trajectory with $r_{p_{\min}} = 0.2$ au and $a_c = 1$ mm/s^2 is shown

a_c [mm/s^2]	$r_{p_{\min}}$ [au]	min(r) [au]	Q-law t_f [years]	t_f from Ref. [58] [years]
0.5	0.1	0.3025	11.9	11.6
	0.2	0.3025	11.9	11.6
	0.3	0.3225	12.2	12.0
	0.4	0.4296	15.0	13.8
1.0	0.1	0.1097	6.9	4.1
	0.2	0.2240	7.9	5.7
	0.3	0.3345	9.0	6.9
	0.4	0.4455	11.0	8.2
2.0	0.1	0.1844	3.3	3.2
	0.2	0.2291	3.6	3.4
	0.3	0.3416	4.5	4.6
	0.4	0.4526	5.5	5.3

Table 1: Comparison between the Neptune flyby-scenario flight times obtained with the Q-law algorithm and literature results [58].

in Fig. 9. In this case, the solar sail-based spacecraft reaches the Neptune's distance, with a flight time of about 7.92 years, after two close passages to the Sun that increase its orbital energy.

To simplify a comparison with the literature results, since the latter are usually given as a function of the minimum Sun-spacecraft distance and not of the perihelion distance as in the Q-law algorithm, Tab. 1 reports

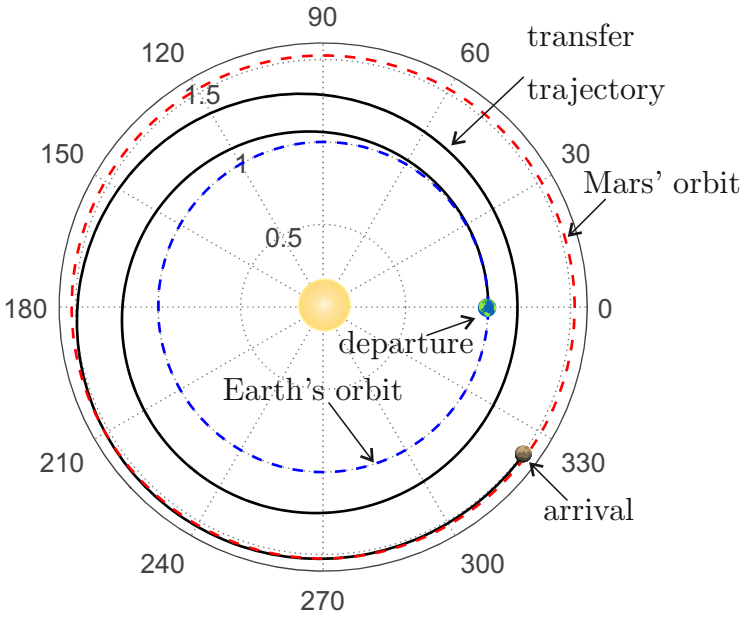

(a) Transfer trajectory. Radial distance in astronomical units.

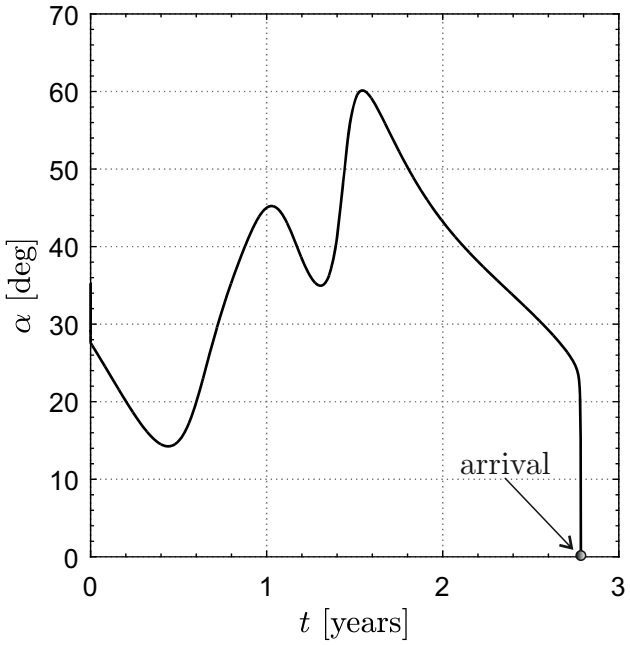

(b) Steering law.

Figure 7: Earth-Mars transfer trajectory when $a_c = 0.3\,\mathrm{mm/s^2}$.

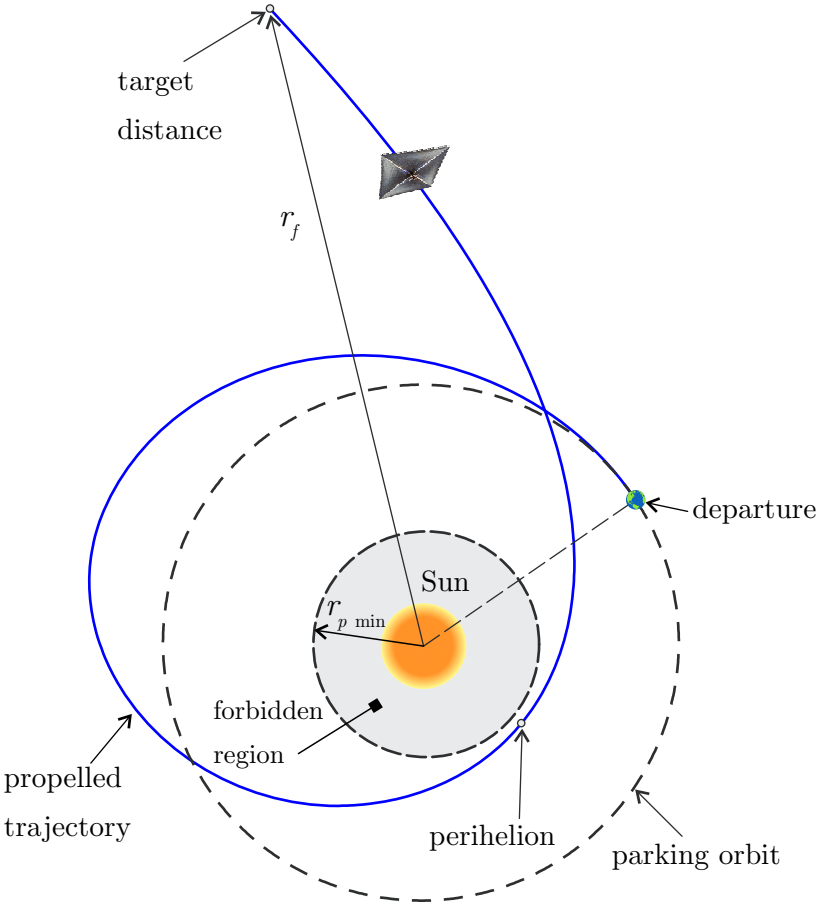

Figure 8: Conceptual sketch of a solar photonic assist maneuver.

the flight times obtained with different values of $r_{p_{\min}}$ and the corresponding minimum values of r obtained along the simulated trajectory. The same table also compares the results with the outputs of an interpolation of data taken from Ref. [58]. In this scenario, the Q-law algorithm provides a very good estimate of the flight times required to reach Neptune's orbit. This is more evident when low-performance solar sails are considered, probably due to the capability of the Q-law algorithm of comprising the possible solar photonic assist maneuvers in the trajectory, a feature that is usually difficult to manage with conventional optimization methods [57].

5. Conclusions

A method for providing a quick approximation of the minimum-time transfer trajectory of a solar sail-based spacecraft has been discussed. The procedure is based on the use of the Q-law algorithm, which is here specialized to the solar sail case by accounting for the thrust dependance on the Sun-spacecraft distance and on the sail attitude.

In particular, the Q-law algorithm approach has been applied to two potential mission cases, that is, an interplanetary transfer and a mission to the outer Solar System region. The algorithm proves to be effective in estimating the minimum flight time required to reach the target, even when compared to the outputs of a global optimization method. The Q-law algorithm is also able to approximate an escape trajectory with multiple photonic assist maneuvers, which are usually difficult to analyze with conventional optimization algorithms. Future investigations will concentrate on considering the effects of perturbative sources, such as third-body gravitational perturbations, in the mathematical formulation of the Q-law algorithm. A further

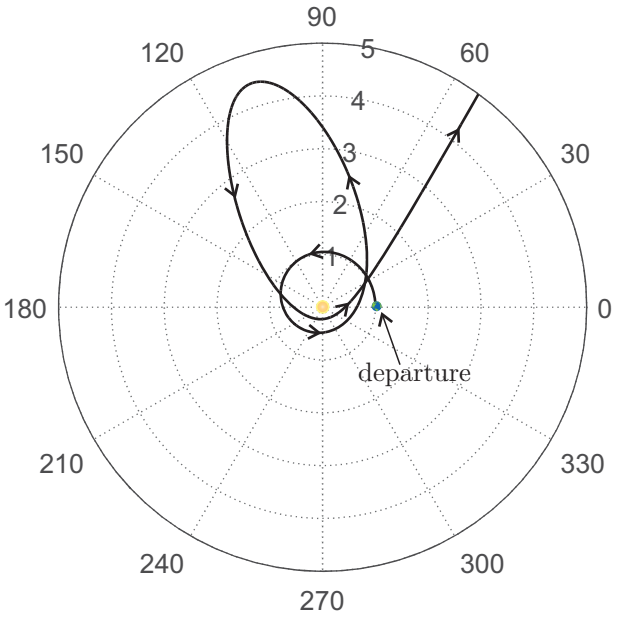

Figure 9: Inner part of the transfer trajectory in a Neptune-flyby case with $a_c = 1\,\mathrm{mm/s^2}$ and $r_{p_{\min}} = 0.2\,\mathrm{au}$. Radial distance in astronomical units.

extension of this work is offered by its generalization to solar sail three-dimensional trajectories, which would require the inclusion of other orbital parameters in the definition of the proximity quotient.

References

[1] J. L. Wright, Space Sailing, Gordon and Breach Science Publishers , 1992, pp. 223–233.

[2] C. R. McInnes, Solar Sailing: Technology, Dynamics and Mission Applications, Springer-Praxis Series in Space Science and Technology, Springer-Verlag, Berlin, 1999, Ch. 2, pp. 46–54.

[3] S. Gong, M. Macdonald, Review on solar sail technology, Astrodynamics 3 (2) (2019) 93–125, doi: 10.1007/s42064-019-0038-x.

[4] J. Kang, K.-C. Park, Flexible heliogyro solar sail under solar radiation pressure and gravitational force, Acta Astronautica 179 (2021) 186–196, doi: 10.1016/j.actaastro.2020.10.042.

[5] O. Mori, H. Sawada, R. Funase, T. Endo, M. Morimoto, T. Yamamoto, Y. Tsuda, Y. Kawakatsu, J. Kawaguchi, Development of first solar power sail demonstrator - IKAROS, in: Proceedings of 21st International Symposium on Space Flight Dynamics (ISSFD), Toulouse, France, 2009.

[6] Y. Tsuda, O. Mori, R. Funase, H. Sawada, T. Yamamoto, T. Saiki, T. Endo, J. Kawaguchi, Flight status of IKAROS deep space solar sail demonstrator, Acta Astronautica 69 (9-10) (2011) 833–840, doi: 10.1016/j.actaastro.2011.06.005.

[7] B. Betts, B. Nye, J. Vaughn, E. Greeson, R. Chute, D. A. Spencer, R. W. Ridenoure, R. Munakata, S. D. Wong, A. Diaz, D. A. Stetson, J. D. Foley, J. M. Bellardo, B. A. Plante, Lightsail 1 mission results and public outreach strategies, in: The 4th International Symposium on Solar Sailing, Kyoto Research Park, Kyoto, Japan, 2017.

[8] B. Betts, D. A. Spencer, B. Nye, R. Munakata, J. Bellardo, S. D. Wong, A. Diaz, R. W. Ridenoure, B. A. Plante, J. D. Foley, J. Vaughn, Lightsail 2: Controlled solar sailing using a CubeSat, in: The 4th International Symposium on Solar Sailing, Kyoto Research Park, Kyoyo, Japan, 2017.

[9] Y. Chu, S. Firuzi, S. Gong, Controllable liquid crystal diffractive sail and its potential applications, Acta Astronautica 182 (2021) 37–45, doi: 10.1016/j.actaastro.2021.02.003.

[10] M. Bassetto, A. Caruso, A. A. Quarta, G. Mengali, Optimal steering law of refractive sail, Advances in Space Research 67 (9) (2021) 2855–2864, doi: 10.1016/j.asr.2019.10.033.

[11] L. McNutt, L. Johnson, P. Kahn, J. Castillo-Rogez, A. Frick, Near-earth asteroid (NEA) scout, in: AIAA SPACE 2014 Conference and Exposition, San Diego (CA), 4–7 August, 2014, paper AIAA 2014-4435.

[12] J. B. Pezent, R. Sood, A. Heaton, K. Miller, L. Johnson, Preliminary trajectory design for NASA's Solar Cruiser: A technology demonstration mission, Acta Astronautica 183 (2021) 134–140, doi: 10.1016/j.actaastro.2021.03.006.

[13] T. Okada, Y. Kebukawa, J. Aoki, S. Ulamec, R. Jaumann, J. Matsumoto, H. Yano, T. Iwata, O. Mori, J.-P. Bibring, Science exploration and instrumentation of the OKEANOS mission to a Jupiter Trojan asteroid using the solar power sail, Planetary and Space Science 161 (2018) 99–106, doi: 10.1016/j.pss.2018.06.020.

[14] Y. Takao, O. Mori, M. Matsushita, A. K. Sugihara, Solar electric propulsion by a solar power sail for small spacecraft missions to the outer solar system, Acta Astronautica 181 (2021) 362–376, doi: 10.1016/j.actaastro.2021.01.020.

[15] C. G. Sauer Jr., Optimum solar-sail interplanetary trajectories, in: AIAA/AAS Astrodynamics Conference, San Diego (CA), August 18-20, 1976, paper AIAA 76-792.
[16] G. Mengali, A. A. Quarta, Optimal heliostationary missions of high-performance sailcraft, Acta Astronautica 60 (8–9) (2007) 676–683, doi: 10.1016/j.actaastro.2006.07.018.
[17] A. A. Quarta, G. Mengali, Solar sail missions to Mercury with Venus gravity assist, Acta Astronautica 65 (3–4) (2009) 495–506, doi: 10.1016/j.actaastro.2009.02.007.
[18] A. A. Quarta, G. Mengali, Optimal solar sail transfer to linear trajectories, Acta Astronautica 82 (2) (2013) 189–196, doi: 10.1016/j.actaastro.2012.03.005.
[19] L. Niccolai, A. A. Quarta, G. Mengali, Analytical solution of the optimal steering law for non-ideal solar sail, Aerospace Science and Technology 62 (2017) 11–18, doi: 10.1016/j.ast.2016.11.031.
[20] Y. Song, S. Gong, Solar sail trajectory optimization of multi-asteroid rendezvous mission, Acta Astronautica 157 (2019) 111–122, doi: 10.1016/j.actaastro.2018.12.016.
[21] J. Heiligers, G. Mingotti, C. R. McInnes, Optimal solar sail transfers between Halo orbits of different Sun-planet systems, Advances in Space Research 55 (5) (2015) 1405–1421, doi: 10.1016/j.asr.2014.11.033.
[22] D. Morante, M. Sanjurjo-Rivo, M. Soler, J. M. Sanchez-Perez, Hybrid multi-objective orbit-raising optimization with operational constraints, Acta Astronautica 175 (2020) 447–461, doi: 10.1016/j.actaastro.2020.05.022.
[23] K. Kitamura, K. Yamada, T. Shima, Quasi-time-optimal steering law for low-thrust orbit transfer considering angular momentum and torque constraints, Acta Astronautica 182 (2021) 332–349, doi: 10.1016/j.actaastro.2021.01.008.
[24] G. W. Hughes, C. R. McInnes, Solar sail hybrid trajectory optimization, in: AAS/AIAA Astrodynamics Conference, Quebec City (QC), Canada, July 30 - August 2, 2001.
[25] A. Caruso, L. Niccolai, A. A. Quarta, G. Mengali, Effects of attitude constraints on solar sail optimal interplanetary trajectories, Acta Astronautica 177 (2020) 39–47, doi: 10.1016/j.actaastro.2020.07.010.
[26] A. Caruso, A. A. Quarta, G. Mengali, Comparison between direct and indirect approach to solar sail circle-to-circle orbit raising optimization, Astrodynamics 3 (3) (2019) 273–284, doi: 10.1007/s42064-019-0040-x.
[27] B. Dachwald, Optimization of very-low-thrust trajectories using evolutionary neurocontrol, Acta Astronautica 57 (2–8) (2005) 175–185, doi: 10.1016/j.actaastro.2005.03.004.
[28] H. Peng, X. Bai, Artificial neural network-based machine learning approach to improve orbit prediction accuracy, Journal of Spacecraft and Rockets 55 (5) (2018) 1248–1260, doi: 10.2514/1.A34171.
[29] L. Cheng, Z. Wang, F. Jiang, C. Zhou, Real-time optimal control for spacecraft orbit transfer via multiscale deep neural networks, IEEE Transactions on Aerospace and Electronic Systems 55 (5) (2019) 2436–2450, doi: 10.1109/TAES.2018.2889571.
[30] Y. Song, S. Gong, Solar-sail trajectory design for multiple near-Earth asteroid exploration based on deep neural networks, Aerospace Science and Technology 91 (2019) 28–40, doi: 10.1016/j.ast.2019.04.056.
[31] M. Macdonald, C. R. McInnes, B. Dachwald, Heliocentric solar sail orbit transfers with locally optimal control laws, Journal of Spacecraft and Rockets 44 (1) (2007) 273–276, doi: 10.2514/1.17297.
[32] S. Hokamoto, K. Sachimoto, K. Fujita, Trajectory design of solar sail spacecraft for interplanetary rendezvous missions, Transactions of Space Technology Japan 26 (7) (2009) 37–42, doi: 10.2322/tstj.7.Pd_37.
[33] G. Mengali, A. A. Quarta, Near-optimal solar-sail orbit-raising from low earth orbit, Journal of Spacecraft and Rockets 42 (5) (2005) 954–958, doi: 10.2514/1.14184.
[34] A. E. Petropoulos, Simple control laws for low-thrust orbit transfers, in: AAS/AIAA Astrodynamics Specialists Conference and Exhibit, Big Sky (MN), August 3-7, 2003, paper AAS 03-630.
[35] A. E. Petropoulos, Low-thrust orbit transfers using candidate Lyapunov functions with a mechanism for coasting, in: AIAA/AAS Astrodynamics Specialist Conference and Exhibit, Providence (RI), August 16-19, 2004, paper AIAA 2004-5089.
[36] D. Yang, B. Xu, Y. T. Gao, Optimal strategy for low-thrust spiral trajectories using Lyapunov-based guidance, Advances in Space Research 56 (5) (2015) 865–878, doi: 10.1016/j.asr.2015.05.030.
[37] G. I. Varga, J. M. Sanchez-Perez, Many-revolution low-thrust orbit transfer computation using equinoctial Q-law including J_2 and eclipse effects, in: 6th International Conference on Astrodynamics Tools and Techniques (ICATT), Darmstadtium, 14-17 March, 2016.
[38] D. Yang, B. Xu, L. Zhang, Optimal low-thrust spiral trajectories using Lyapunov-based guidance, Acta Astronautica 126 (2016) 275–285, doi: 10.1016/j.actaastro.2016.04.028.
[39] A. E. Petropoulos, Refinements to the Q-law for low-thrust orbit transfers, in: AAS/AIAA Space Flight Mechanics Meeting, Copper Mountain (CO), January 23-27, 2005, paper AAS 05-162.
[40] A. E. Petropoulos, S. Lee, Optimisation of low-thrust orbit transfers using the Q-law for the initial guess, in: AAS/AIAA Astrodynamics Conference, South Lake Tahoe (CA), August 7–11, 2005, paper AAS 05-392.
[41] S. Lee, A. E. Petropoulos, P. Von Allmen, Low-thrust orbit transfer optimization with refined Q-law and multi-objective genetic algorithm, in: AAS/AIAA Astrodunamics Conference, South Lake Tahoe (CA), August 7–11, 2005, paper AAS 05-393.
[42] J. L. Shannon, M. T. Ozimek, J. A. Atchison, C. M. Hartzell, Q-law aided direct trajectory optimization of many-revolution low-thrust transfers, Journal of Spacecraft and Rockets 57 (4) (2020) 672–682, doi: 10.2514/1.A34586.
[43] C. R. McInnes, Delivering fast and capable missions to the outer solar system, Advances in Space Research 34 (1) (2004) 184–191, doi: 10.1016/j.asr.2003.02.063.
[44] C. G. Sauer Jr., Solar sail trajectories for solar polar and interstellar probe missions, Advances in the Astronautical Sciences [also paper AAS 99-336]. 103 (1) (2000) 1–16 .
[45] X. Zeng, K. T. Alfriend, J. Li, S. R. Vadali, Optimal solar sail trajectory analysis for interstellar missions, Journal of the Astronautical Sciences 59 (3) (2012) 502–516, doi: 10.1007/S40295-014-0008-y.
[46] M. Leipold, O. Wagner, 'Solar photonic assist' trajectory design for solar sail missions to the outer solar system and beyond, in: AAS/GSFC International Symposium on Space Flight Dynamics, Greenbelt (MD), May 11–15, 1998.

[47] M. Leipold, H. Fichtner, B. Heber, P. Groepper, S. Lascar, F. Burger, M. Eiden, T. Niederstadt, C. Sickinger, L. Herbeck, B. Dachwald, W. Seboldt, Heliopause Explorer-A sailcraft mission to the outer boundaries of the solar system, Acta Astronautica 59 (8–11) (2006) 785–796, doi: 10.1016/j.actaastro.2005.07.024.
[48] A. A. Quarta, G. Mengali, Electric sail mission analysis for outer solar system exploration, Journal of Guidance, Control, and Dynamics 33 (3) (2010) 740–755, doi: 10.2514/1.47006.
[49] G. Mengali, A. A. Quarta, C. Circi, B. Dachwald, Refined solar sail force model with mission application, Journal of Guidance, Control, and Dynamics 30 (2) (2007) 512–520, doi: 10.2514/1.24779.
[50] B. Dachwald, G. Mengali, A. A. Quarta, M. Macdonald, Parametric model and optimal control of solar sails with optical degradation, Journal of Guidance, Control, and Dynamics 29 (5) (2006) 1170–1178, doi: 10.2514/1.20313.
[51] B. Dachwald, M. Macdonald, C. R. McInnes, G. Mengali, A. A. Quarta, Impact of optical degradation on solar sail mission performance, Journal of Spacecraft and Rockets 44 (4) (2007) 740–749, doi: 10.2514/1.21432.
[52] A. Tessler, D. W. Sleight, J. T. Wang, Effective modeling and nonlinear shell analysis of thin membranes exhibiting structural wrinkling, Journal of Spacecraft and Rockets 42 (2) (2005) 287–298, doi: 10.2514/1.3915.
[53] G. Vulpetti, D. Apponi, X. Zeng, C. Circi, Wrinkling analysis of solar-photon sails, Advances in Spade Research 67 (9) (2021) 2669–2687, doi: 10.1016/j.asr.2020.07.016.
[54] G. Mengali, A. A. Quarta, Rapid solar sail rendezvous missions to asteroid 99942 apophis, Journal of Spacecraft and Rockets 46 (1) (2009) 134–140, doi: 10.2514/1.37141.
[55] A. A. Quarta, G. Mengali, L. Niccolai, Solar sail optimal transfer between heliostationary points, Journal of Guidance, Control, and Dynamics 43 (10) (2020) 1935–1942, doi: 10.2514/1.G005193.
[56] M. Huo, G. Mengali, A. A. Quarta, Mission design for an interstellar probe with e-sail propulsion system, JBIS: Journal of the British Interplanetary Society 68 (5-6) (2015) 128–134 .
[57] M. Bassetto, A. A. Quarta, G. Mengali, Locally-optimal electric sail transfer, Proceedings of the Institution of Mechanical Engineers, Part G: Journal of Aerospace Engineering 233 (1) (2019) 166–179, doi: 10.1177/0954410017728975.
[58] B. Dachwald, Optimal solar-sail trajectories for missions to the outer solar system, Journal of Guidance, Control, and Dynamics 28 (6) (2005) 1187–1193, doi: 10.2514/1.13301.